Ocean Engineering 288 (2023) 116135

Contents lists available at ScienceDirect

Ocean Engineering

journal homepage: www.elsevier.com/locate/oceaneng

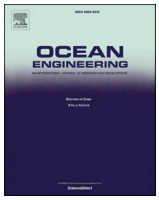

Rigorous SIF-based prediction of fatigue life improvement for prestressed-CFRP-repaired cracked steel plates

Yu Zhang [a,*], Feifan Zhang [a], Zhansheng Guo [b], Nao-Aki Noda [c,**]

[a] College of Safety and Ocean Engineering, China University of Petroleum, Beijing, 102249, China
[b] Tianjin Fire Science and Technology Research Institute of MEM, Tianjin, 300381, China
[c] Mechanical Engineering Department, Kyushu Institute of Technology, Fukuoka, 804-8550, Japan

ARTICLE INFO

Handling Editor: Prof. A.I. Incecik

Keywords:
Fatigue life improvement
Carbon fiber reinforced polymer
Cracked steel plate
Crack propagation
Prestress

ABSTRACT

Carbon fiber reinforced polymer (CFRP) can be widely used to repair damaged plates in marine engineering equipment. To predict the fatigue life improvement by this repair, the stress intensity factor (SIF) of the cracked plate without/with repair is analyzed rigorously. Specifically, the SIF of a cracked plate without repair is analyzed and the error due to the finite element model (FEM) mesh is evaluated by comparing with the exact solution. By applying the same mesh having the same error, the exact SIF of the repaired plate is obtained in a convenient form. Fatigue experiments reveal that the same crack propagation parameters (C and m) can be applied for the unrepaired/repaired plates. Based on those, the prediction equation of fatigue life is obtained for cracked steel plates repaired with prestressed CFRP. The results show that this prediction method has the advantages of simplicity and efficiency.

1. Introduction

Steel construction, which is utilized in offshore engineering equipment, has comprehensive advantages of factory manufacturing, fast installation, short construction period, good seismic performance, and fast investment recovery. In offshore engineering equipment, Steel plates are the most common and widely utilized in steel structures. Those marine structures and ocean engineering are subjected to fatigue loads, such as wind, wave and current, which could cause cracks in these steel structures, and the cracks may propagate even fracture. Typical repair methods for cracked plates are grinding, welding, fixture, and composite repair (Al-Karawi et al., 2020; Mazaheri et al., 2021; Russian et al., 2022). Among them, the composite repair is widely used not only for repair but for maintenance because it is low cost, relatively easy to process, and can be completed in a short time. Composite repair techniques were originally used to reinforce concrete structures. With the advancement of technology, they are becoming more and more diverse. The repairing of damaged marine structures and equipment with composite material is widely used as shown in Fig. 1-Fig. 3, such as repairing cracked steel plates on FPSO, repairing corroded deck on FOU, repairing semi-submersible platform ballast tank (Weitzenboeck and Mcgeorge, 2012) (see Fig. 2).

In the previous studies, Liu et al. (2009) studied the parameters of thickness, length, and structural configuration of the patch, had a significant impact on fatigue life extension of cracked steel plate for repairs utilizing single-sided and double-sided CFRP. For reinforced concrete beams strengthened with prestressed CFRP, Xue et al. (2010) noted out that compression damage, tensile damage, and debonding damage may be the potential bending damage modes, and estimated the flexural strength of the beams under the respective damage modes. In addition, the presence of prestressed CFRP was considered in the prediction of cracking moment, crack width, and deflection of reinforced beams. Wu et al. (2012) investigated the fatigue performance of cracked steel plates fixed using CFRP with an ultra-high modulus. The impacts of CFRP bond length, bond width, and bond placement were considered. A comparison of the strengthening effect of normal Young's modulus, high Young's modulus and ultra-high modulus CFRP plates with and without prestressing was also carried out. Yu et al. (2014) evaluated the fatigue performance of cracked steel plates with varying degrees of initial damage and discovered that employing ultra-high modulus CFRP laminates and fixing at an incipient stage resulted in more efficient strengthening. Kafodya et al. (2015) investigated the durability of pultruded unidirectional CFRP plates submerged in water and saltwater at room temperature and subjected to prolonged bending strains of various ultimate strain, and the mechanisms of CFRP strength degradation was

* Corresponding author.
** Corresponding author.
E-mail address: zhangyu@cup.edu.cn (Y. Zhang).

https://doi.org/10.1016/j.oceaneng.2023.116135
Received 16 August 2023; Received in revised form 7 October 2023; Accepted 21 October 2023

Nomenclature

a	Crack length (mm)
C	Material constants
m	Material constants
W	Width of steel plate (mm)
N	Number of cyclic
$N_{c\text{-}un}$	the number of cycles to failure for unrepaired steel plates
$N_{c\text{-}\sigma p}$	the number of cycles to failure for repaired steel plates
K_{fc}	Fracture toughness (MPa•mm$^{1/2}$)
R	stress ratio
σ	Stresses loaded at both ends of the plate (MPa)
σ_p	Prestress (MPa)
F_{1-un}^{FEM}	Dimensionless SIFs of the unrepaired steel plate obtained by FEM
F_{1-0}^{FEM}	Dimensionless SIFs of the steel plate repaired with normal CFRP by FEM
$F_{1-\sigma_p}^{FEM}$	Dimensionless SIFs of the steel plate repaired with prestressed CFRP by FEM
K_{1-un}^{FEM}	SIFs of the unrepaired steel plate obtained by FEM (MPa•mm$^{1/2}$)
K_{1-0}^{FEM}	SIFs of the steel plate repaired with normal CFRP by FEM (MPa•mm$^{1/2}$)
$K_{1-\sigma_p}^{FEM}$	SIFs of the steel plate repaired with prestressed CFRP by FEM (MPa•mm$^{1/2}$)
σ_{z-un}^{FEM}	the FEM stress at the crack tip of the unrepaired specimen (MPa)
σ_{z-0}^{FEM}	the FEM stress at the crack tip of the specimen repaired with normal CFRP (MPa)
$\sigma_{z-\sigma_p}^{FEM}$	the FEM stress at the crack tip of the specimen repaired with prestressed CFRP (MPa)
F_{1-un}^{EXACT}	the exact dimensionless SIF of the unrepaired steel plate
F_{1-0}^{EXACT}	the exact dimensionless SIF of the steel plate repaired with normal CFRP
$F_{1-\sigma_p}^{EXACT}$	the exact dimensionless SIF of the steel plate repaired with prestressed CFRP
K_{1-un}^{EXACT}	the exact SIF of the unrepaired steel plate (MPa•mm$^{1/2}$)
K_{1-0}^{EXACT}	the exact SIF of the steel plate repaired with normal CFRP (MPa•mm$^{1/2}$)
$K_{1-\sigma_p}^{EXACT}$	the exact SIF of the steel plate repaired with prestressed CFRP (MPa•mm$^{1/2}$)

Subscripts

max	maximum
min	minimum

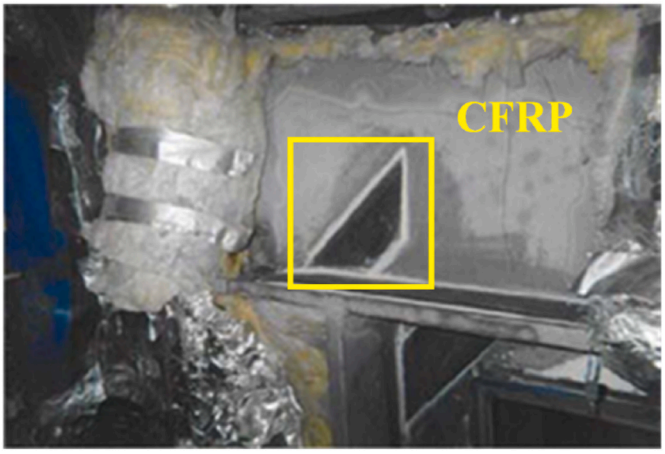

Fig. 1. Repairing cracked steel plates on FPSO with CFRP.

Fig. 2. Repairing corroded deck on FOU with CFRP.

studied. Al-Mosawe et al. (2016) found a considerable in bond strength reinforcement under impact load, while the effective bond length was largely unaffected by high loading rates. Batuwitage et al. (2017) proposed a parametric study to explore the effect of surface preparation process for steel plate, primer, number of CFRP layers and exposure duration in corrosion conditions on the failure modes and tensile capacity of double strap joints. Pang et al. (2019) conducted an experiment to investigate the bonding behavior of the CFRP-steel interface under quasi-static cyclic loading, and researched the effects of bond length, adhesive thickness, adhesive type and loading protocols on it. Liu et al. (2021) presented a novel CFRP-steel tube composite member to prevent debonding failure, and studied the strengthening impact of length of the thick-walled tube and the number of CFRP layers on the peak bearing capacity and the maximum ductile displacement.

The safety and reliability of the repaired structure depends on their fatigue performance. Ineffective fatigue performance can lead to wasted resources and continued failure of refurbished steel plate, substantial financial losses and serious safety hazards (Colombi and Fava, 2016; Orcesi et al., 2019). Therefore, it is of great significance to investigate the fatigue performance of cracked steel plates repaired with composite materials during fatigue loadings. Several studies are focusing on the fatigue performance. Täljsten et al. (2009) evaluated the fatigue performance of structures repaired with non-prestressed and prestressed CFRP by conducting fatigue tensile tests on aged steel plates with central crack. The findings suggested that when non-prestressed CFRP was utilized, fatigue life can be greatly increased, while crack extension appears to be totally stopped when prestressed laminates were employed. Feng et al. (2014) studied the fatigue performance of CFRP reinforced cracked steel plates at various temperatures. The present analytical approach for forecasting the fatigue life of composite structure when temperature effects were considered has been enhanced in this research, and it was also confirmed by the corresponding

Fig. 3. Repairing semi-submersible platform ballast tank with CFRP.

experiments. Li et al. (2019) demonstrated that double-sided repair with CFRP was more efficient than single-sided repair. When utilized with prestressed CFRP, the effect was further enhanced. A larger prestress level resulted in a bigger improvement in fatigue life of central inclined cracked steel plate. Liu et al. (2019) devised a useful SIF method for forecasting the fatigue life of center cracked steel plate through a series of finite element case analyses, which results were confirmed by comparison with test results in various papers. Cabrilo et al. (2019) used the SIF formula and the Paris-Erdogan formula to evaluate the fatigue crack propagation rate in the base metal, heat affected zone, and welded metal zone to investigate the fatigue performance of welded armor steel. Chen et al. (2020) looked at the effectiveness of CFRP for improving the fatigue performance of porous crack-containing steel plates, as well as the influence of hole size and placement on repair efficiency. CFRP repair may enhance the fatigue life of porous broken steel plates to the same level as centrally cracked plates, according to the findings. Considering the effects of initial crack depth, CFRP modulus, CFRP thickness and residual stress of welding, Jie et al. (2020) examined the range of SIFs for unrepaired and cruciform welded joints repaired with CFRP, fitted a new equation to calculate the range of SIFs based on numerical results, and predicted the fatigue life using a modified Paris equation, which correlated well with the experimental results. Hassan et al. (2021) fabricated several sets of standard fatigue test specimens to test the fatigue performance of cracked steel plates with different reinforcement configurations, repair schemes and initial crack lengths, and also observed the development of debonding in composite structures. Lepretre et al. (2021) evaluated SIF for metal plates with a crack emanating from the central hole using the virtual crack closure technique, taking account the effects of different reinforcing configurations and CFRP types. Experiments were used to verify the correctness of the crack extension FEA, and a parametric analysis of the fatigue performance impacted by prestressing on CFRP was carried out. The results show that prestressing is a powerful reinforcing choice. Tan et al. (2021) created a local model of steel joists with integral nodes and a FEM of steel truss bridges to assess the fatigue life. Combining the SIF equation and the Paris-Erdogan equation allowed them to analyze the initial crack propagation and forecast the remaining life. To obtain a model for the corrosion-fatigue life prediction of reinforced concrete square piles in marine environments, Shao et al. (2022) developed a crack growth model based on the Paris-Erdogan equation. He utilized an example to demonstrate the model's validity and performed a parametric analysis of the key influencing factors. Wang et al. (2023) created a novel prestressing system using CFRP for the reinforcement of damaged steel beams. The effects of bonding layer, prestressing level and CFRP plate area on the reinforcement efficiency were investigated and subsequently parametrically analyzed by using finite element modeling, which showed that the reinforcement efficiency increased with the increase of the prestressing level. Liu et al. (2023) proposed an extended finite element analysis model considering various stages of crack propagation and verified its validity with comparative analysis with experimental data, which showed that the model can reasonably predict the fatigue performance of center-cracked steel plates reinforced with partially covered CFRP. Deng et al. (2023) used a combination of shape memory alloy (SMA) and CFRP to achieve hybrid self-prestressing reinforcement for fatigue cracks. Static and fatigue tensile tests revealed that SMA/CFRP composite reinforcement can effectively retard steel cracking and provide better strengthening than CFRP alone.

As mentioned above, several previous studies discussed the fatigue life by fatigue testing and the SIF analysis for unrepaired/repaired structures. However, there was no detail discussion for the accuracy of the SIF formula, and the useful method was not proposed to predict the fatigue life of these structures. Since the steel plates repaired with CFRP is now widely used because of their advantages, the fatigue life prediction has been requested to evaluate the safety. This paper experimentally investigates the fatigue performance of cracked steel plates repaired with conventional CFRP firstly. Referring to test specimens, a series of FEMs, including unrepaired and repaired steel plates, were constructed to analyze the SIF. The errors due to the FEM mesh were evaluated by comparing with the numerical solution. The exact SIF of repaired plates were obtained through proportional method. Based on the rigorous SIF, the significant parameters C and m of crack propagation were gained. The fatigue life prediction equations for cracked steel plates with different repair configurations were built. The numerical method and experimental results were used to evaluate the fatigue life of repaired plates, with good consistency. This numerical method can also be utilized to predict the fatigue life of steel plates repaired with CFRP considering the effect of prestress.

2. Fatigue experiment of cracked plate repaired by CFRP

2.1. Fatigue experiment model

To investigate the efficiency of CFRP repair on prolonging fatigue life, fatigue tests were conducted on cracked steel plates unrepaired and repaired with CFRP. It is crucial to obtain the real mechanical property parameters of the steel plate. Fig. 4 shows the geometry and dimensions

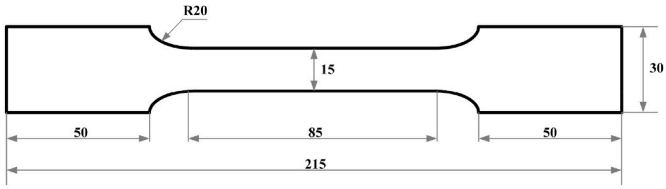

Fig. 4. The Q235 steel specimen used for investigating material properties Table 1 (unit: mm).

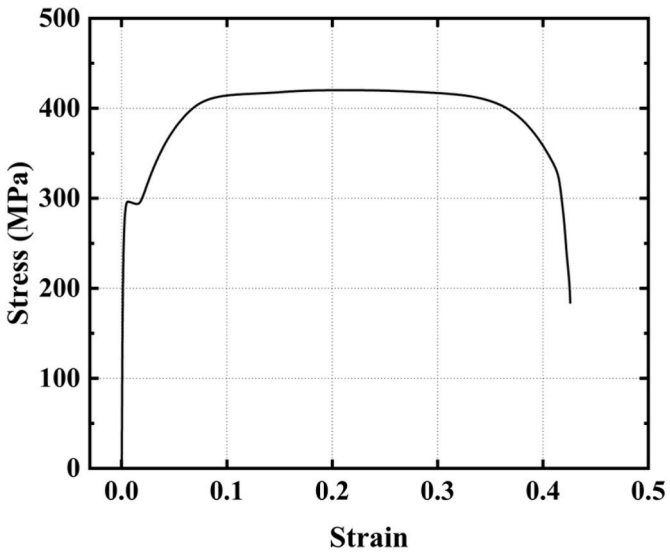

Fig. 5. Nominal stress versus strain curves.

Table 1
The main mechanical properties of Q235.

Young's modulus (GPa)	Yield strength (MPa)	Tensile strength (MPa)	Poisson's ratio	Fracture toughness ($MPa\bullet m^{1/2}$)	Fatigue crack growth threshold ($MPa\bullet m^{1/2}$)
206	297	420	0.3	83.16	6.424

of the tensile specimen used to obtain mechanical properties based on National Standard of China (GB/T 228.1–2021, 2022). Fig. 5 shows the nominal stress versus strain curves of Q235. Table 1 presents the mechanical properties of Q235 obtained according to Fig. 4, fracture toughness (Li et al., 2022) and fatigue crack growth threshold (Dong and Mei, 2003).

In this study, the fatigue crack propagation pattern will be investigated to clarify the effect of repaired by CFRP. Fig. 6 shows the cracked steel plate specimen subjected to cyclic tensile loading without repairing. The specimens were designed considering the stress intensity factors where the steel plate width W is 10 times larger than the initial crack length $2a$.

Liu et al. (2009) investigated the effective repair length and the effective number of layers of CFRP reinforcement, the results showed that the length of CFRP exceeding 50% of the total length of specimen was sufficient and that five layers of CFRP were sufficient to meet the repair expectations. Aljabar et al. (2018) evaluated the fatigue life enhancement of single- and double-sided CFRP repairs; the results showed that the double-sided CFRP repair is much more useful than the single-sided CFRP repair. According to these references, the length of the CFRP in the fatigue test was determined to be 250 mm with a width of 70 mm, and five layers were stacked with a thickness of 0.22 mm per layer and pasted on the upper and lower planes of the cracked steel plate, as illustrated in Fig. 7. The laying angles of the fibers are 0°, 45°, 90°, −45°, 0°. The dimensions of the specimens are shown in Table 2. Table 3 shows material properties of CFRP T700 provided by the manufacturers.

The cracked steel plate specimen shown in the upper panel of Fig. 8. For the repairment, the surface was firstly descaled and the CFRP bonded region was sanded, the five CFRP layers were bonded together, and cured together at room temperature. The cured CFRP sheets were then bonded to the surface of the steel plate. Finally, the bonded specimens were cured for 7 days at room temperature about 20 °C. The repaired specimen is shown in Fig. 8. Table 4 shows the mechanical properties of adhesive Araldites® 2015 provided by manufacturers.

The remote tensile stress σ is applied so that the maximum stress $\sigma_{max} = 178$ MPa, which does not exceed 60% of the steel yield strength. The stress ratio R is fixed as $R = 0.1$ at a frequency of 10Hz. The experiments were conducted on the MTS LFV500-T5000 Nm fatigue testing machine until fracture occurred and each unrepaired and repaired fatigue specimen is tested two times. Fig. 9 depicts the experimental set-up. To track the crack propagation, so-called beach marking method is used by inserting smaller stress amplitude cycles with limited number of cycles to the original applied cyclic loading. Fig. 10 illustrates the beach mark loading with the stress ratio $R = 0.55$ with a frequency of 10Hz. For unrepaired plates, after the 30000 cycles of fatigue load, the 15000 cycles of beach marking load are added. While for repaired plates cycles of fatigue load are 60000, and the cycles of marking load was 30000, the other load setting stayed the same.

2.2. Experimental results

The loading of the fatigue testing machine makes the specimen undergo crack propagation until fracture. The fractured central cross section of the unrepaired specimen is shown as Fig. 11. In smooth surface regions, beach marks are seen as extensions of stable fatigue cracks. The rough region indicates final unstable fracture. From Fig. 11, the critical crack length where unstable fracture occurs can be determined as $2a_{c\text{-}un} = 44.10$ mm for the unrepaired specimen.

The fractures central cross section of the repaired specimen is shown as Fig. 12. In smooth surface regions, beach marks can be also observed as the fatigue crack extension. Compared to Fig. 11, the rough region where the final unstable fracture happened is comparatively smaller and the stable fatigue crack extension region is larger due to the CFRP reinforcement. From Fig. 12, the critical crack length can be determined as $2a_{c\text{-}0} = 53.00$ mm for the repaired specimen with zero prestress.

The relation between the crack length and the number of cycles experimentally obtained by using beach marking method, as presented in Fig. 13. The labels C1and D1 in the figure indicate the unrepaired and

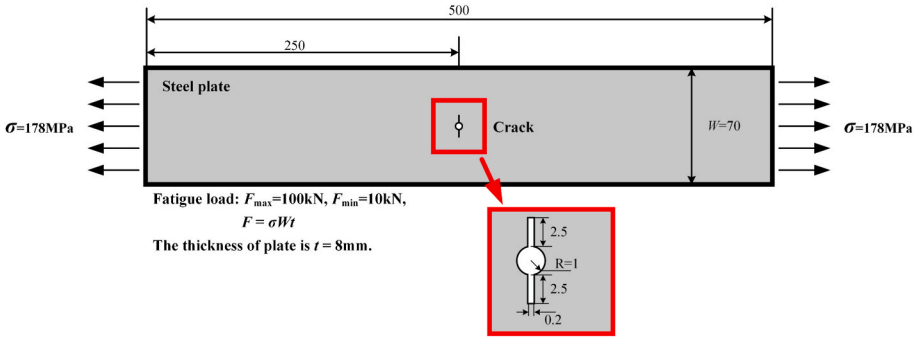

Fig. 6. Schematic illustration of cracked steel plate without repair (unit: mm).

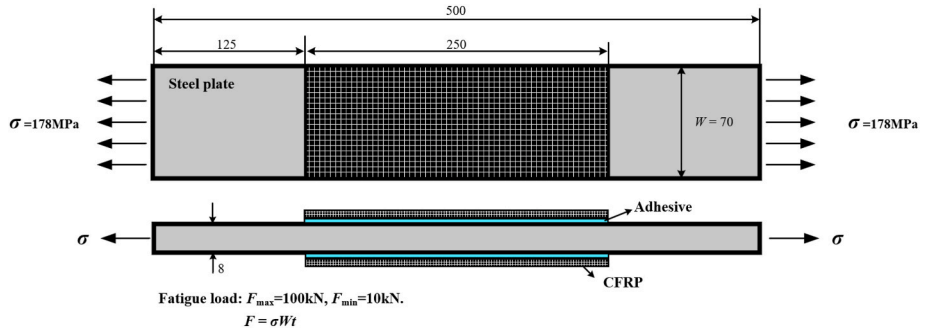

Fig. 7. Schematic illustration of cracked steel plate repaired by CFRP (unit: mm).

Table 2
Dimensions of the specimen.

Specimen	Length L (mm)	Width W (mm)	Thickness t (mm)
Steel plate	500	70	8
CFRP	250	70	1.1 (0.22 × 5)

Table 3
Material properties of CFRP.

Density (g/cm^3)	Young's Modulus (GPa)	Shear Modulus (GPa)	Poisson's Ratio	Thermal expansion coefficient (/°C)
1.76	$E_1 = 233$, $E_2 = 23.1$, $E_3 = 23.1$	$G_{12} = 27.58$, $G_{13} = 27.58$, $G_{23} = 5.89$	$\mu_{12} = 0.34$, $\mu_{13} = 0.28$, $\mu_{23} = 0.28$	$\alpha_{11} = -0.7 \times 10^{-6}$

steel plates repaired with CFRP, respectively, consistent with Figs. 8−1 and −2 represent the first and the second specimen of each type to have the mean experimental values. The labels in the subsequent figures represent the same meaning. Focusing on the end point where final unstable fracture occurs, the critical crack length is extended by 1.2 times by the CFRP repair and the number of cycles to failure is extended by 2.37 times by the CFRP repair. The experiments have demonstrated that CFRP repair is effective in improving the fatigue life of cracked steel plates. The experiments have demonstrated that CFRP repair is effective in improving the fatigue life of cracked steel plates, which is consistent the fatigue experiments conducted by (Lepretre et al., 2021), and it was proved that the presence of CFRP inhibited crack opening and thus reduced fatigue crack propagation rate.

The final crack length and number of load cycles to failure and the fracture toughness for the unrepaired/repaired specimens by using SIF equation discussed later are summarize in Table 5. The fatigue fracture toughness of the unrepaired steel plate can be obtained as $K_{fc} = 63.02$ MPa m$^{1/2}$ from the final crack length $2a_{c\text{-}un} = 44.10$ mm and the SIF solution for Fig. 6. Also, the fatigue fracture toughness of the repaired steel plate can be obtained as $K_{fc} = 55.31$ MPa m$^{1/2}$ from the final crack length $2a_{c\text{-}0} = 53.00$ mm and the SIF results analytically obtained for the repaired plate in Fig. 7. Compared to the average fracture toughness K_{fc} of unrepaired steel plates, the relative error of the fracture toughness K_{fc} obtained through repaired steel plates was 12.24%. This difference can be explained from the extension of the delamination area of the CFRP repair plate. This difference can be explained from the extension of the delamination area of the CFRP repair plate (Lepretre et al., 2021).

2.3. Finite element model

Finite element software, Abaqus (2020), was applied for investigating the SIF of unrepaired/repaired specimens and thus analyzing the correlation between the crack extension length and the number of load cycles (a-N). A series of FEMs were constructed to obtain the SIF for different crack lengths. Fig. 14 shows as example of FEM mesh constructing a contour integral region at the tip of the crack. The element type is C3D6 (6-node tetrahedral 3D stress element type) used for contour integral region are indicated by yellow circles, and the element type is C3D8 (8-node hexahedral 3D stress element type) are used for other regions. The element type used for CFRP in the repair structure is also C3D8. In addition, the cohesive model was applied to model the interfacial adhesion region. The bilinear model was employed to characterize the cohesive model, in which the key parameters are shown in Table 4.

In previous studies, it was discovered that the configuration of prestress was employed as a technique to improve repair performance of CFRP. In this study, several analyses were carried out to examine the effect of prestress on the mechanical and fatigue characteristics of repaired structures. Under a load of 60% yield strength, the axial displacement of a cracked steel plate is determined to be 0.22 mm. Furthermore, the existence or absence of prestress distinguishes the condition of the CFRP, with prestress $\sigma_p = 10$, 20, 30, 40, 50, 80 and 100 MPa. The techniques for introducing prestress on CFRP are often directly applying and temperature effect. The temperature rise approach is employed to produce the prestress in this investigation. The coefficients of thermal expansion are shown in Table 3. The dimensions of the FE models are same with Table 2, where the boundary conditions are added to the model using a setup with loading ($\sigma = 178$ MPa) at one end and fixed constraints at the other. The numerical matrix is presented in Table 6.

The variation of the SIF with increasing the total number of the mesh by varying element size is depicted in Fig. 15 when the crack length $a = 3.5$ mm ($2a/W = 0.1$). By averaging the values of the six element nodes in the direction of the plate's thickness, the specific value of SIF for crack tip is determined. In Fig. 15, the CPU time is also indicated as a dotted line with the red figure showing the number of elements on the integral path. As shown in Fig. 15, when the total element number is less than 32000 and the element number on the integral path is less than 90, the SIF is still slightly increasing with increasing the mesh. However, when the total number of the mesh is larger than 32000, the real calculation times needs more than a few days by using the computer currently used (DESKTOP-3O0CATT, CPU: AMD Ryzen 5 3500X 6-Core Processor 3.59 GHz, Memory: 16 GB). Such calculation time is not suitable for systematic calculation for various crack lengths and various repair conditions. Therefore, the following systematic calculations will be performed

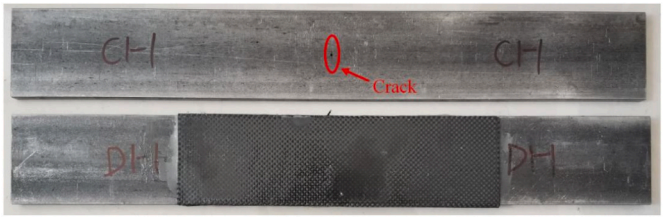

Fig. 8. Test specimens, C1 (up) and D1 (down).

Table 4
Mechanical properties of adhesive.

Young's Modulus (GPa)	Shear Modulus (GPa)	Poisson's Ratio	Tensile yield strength (MPa)	Tensile failure strength (MPa)	Shear yield strength (MPa)	Shear failure strength (MPa)
1.80	0.68	0.33	12.63	21.63	14.6	17.9

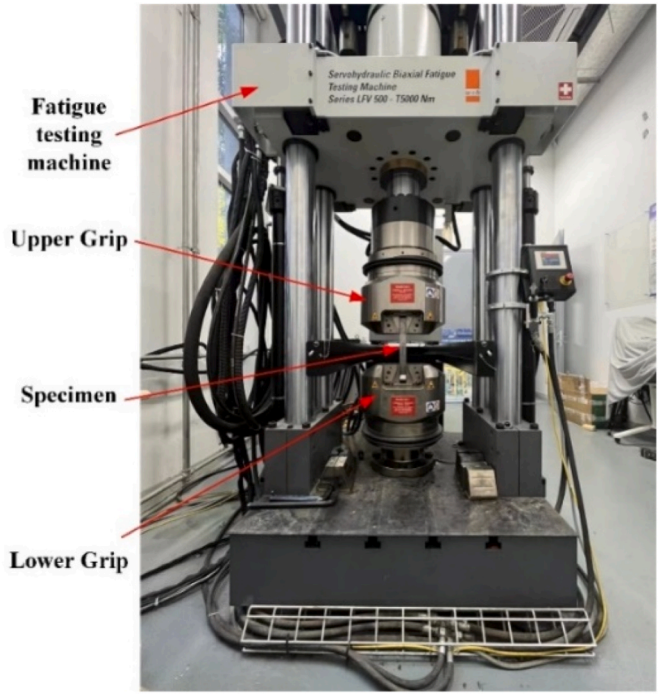

Fig. 9. Experimental setup.

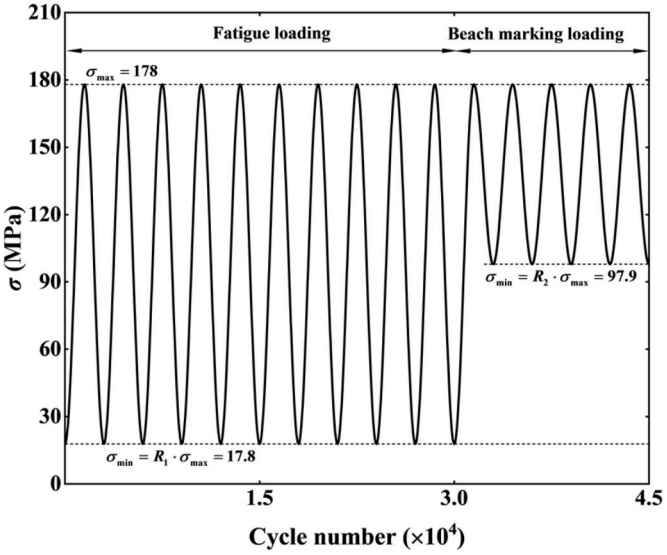

Fig. 10. Test stress range of "Beach Marking" technique.

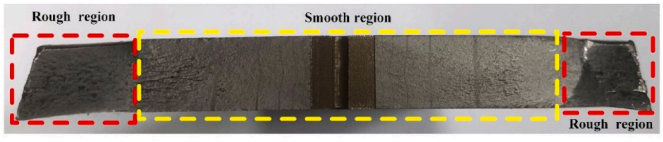

Fig. 11. Fractured central cross section of the unrepaired specimen.

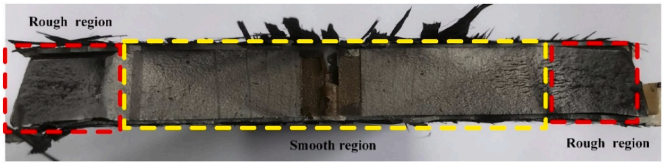

Fig. 12. Fractured central cross section of the repaired specimen.

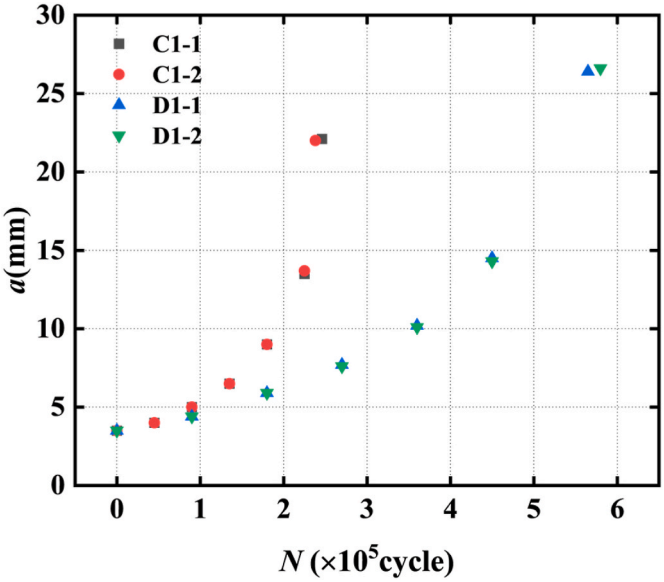

Fig. 13. Crack length a versus number of cyclic N experimentally obtained by using beach marking method.

Table 5
Critical crack length, number of cycles to failure and fatigue fracture toughness of specimens in Figs. 11 and 12.

Specimen number	Final crack length $2a$ (mm)	Average value $2a$ (mm)	Fatigue fracture toughness K_{fc} calculated by Eq. (4) (5) (MPa•m$^{1/2}$)	Number of cycles to failure N (10^6)	Average values of N (10^6)
C 1-1	44.20	44.10	63.02	0.246	0.242
C 1-2	44.00			0.238	
D 1-1	52.80	53.00	55.31	0.565	0.5725
D 1-2	53.20			0.580	

3Rigorous FEA for SIF of cracked plate repaired by prestressed CFRP.

by using the mesh when the total number of the mesh is about 24000 with the element number 64 on the integral path. As will be discussed later, the values of the SIF may have some errors less than 10%, the correction method will be shown in section 4 based on the idea of proportional stress fields.

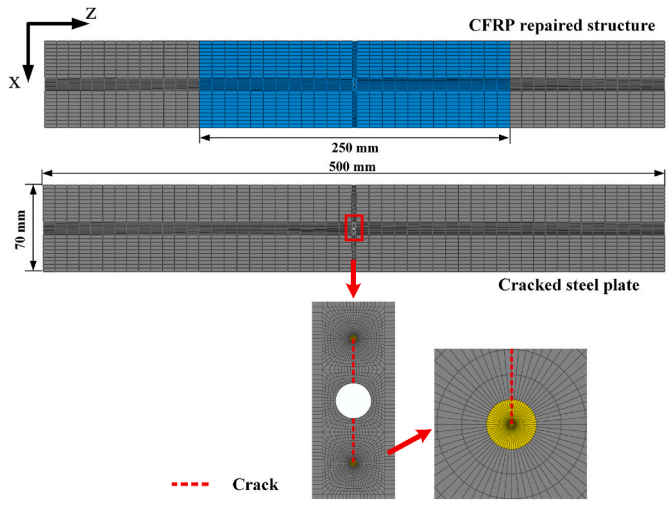

Fig. 14. FEM mesh to calculate SIF whose yellow circle shows a path for the contour integral method installed in Abaqus.

Table 6
Numerical test matrix for SIF analysis.

Configuration	Half crack length (a/mm)	Prestress (σ_p/MPa)
Unrepaired	3.5, 4, 5, 7, 9, 11, 13, 15, 17, 19, 21, 23, 25, 27	N/A
Repaired with CFRP	3.5, 4, 5, 7, 9, 11, 13, 15, 17, 19, 21, 23, 25, 27	0, 10, 20, 30, 40, 50, 80, 100

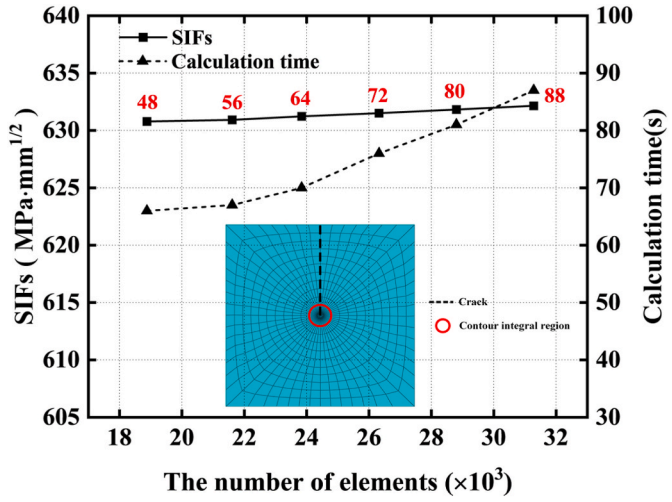

Fig. 15. Influence of the element numbers on the integration path on SIF and calculation time.

2.4. The proportional method for correcting SIF

The dimensionless SIFs $F_1^{FEM} = K_1^{FEM}/(\sigma\sqrt{\pi a})$ obtained by the contour integral method installed in Abaqus is exhibited in Table 7 when the relative crack length $2a/W$ = 0.1, 0.2, 0.6, 0.7714. F_{1-un}^{FEM} denotes the dimensionless SIF of the unrepaired specimen. And, notations F_{1-0}^{FEM}, F_{1-50}^{FEM}, F_{1-100}^{FEM} denote the dimensionless SIFs of the repaired specimens when the prestress σ_p = 0, 50, 100 MPa, respectively. The SIF ratios $F_{1-0}^{FEM}/F_{1-un}^{FEM}$, $F_{1-50}^{FEM}/F_{1-un}^{FEM}$, $F_{1-100}^{FEM}/F_{1-un}^{FEM}$ are also indicated in the parenthesis just below the value of F_{1-0}^{FEM}, F_{1-50}^{FEM}, F_{1-100}^{FEM}, respectively.

Similarly, the FEM stress value at the crack tip (see Fig. 14) of the unrepaired specimen is indicated as σ_{z-un}^{FEM}. Also, σ_{z-0}^{FEM}, σ_{z-50}^{FEM}, σ_{z-100}^{FEM} denote the stress at the crack tip of the repaired specimen obtained by the FEM when the prestress σ_p = 0, 50, 100 MPa, respectively. All values are obtained from the same mesh node of the crack tip of different models. Then, the FEM stress ratios $\sigma_{z-0}^{FEM}/\sigma_{z-un}^{FEM}$, $\sigma_{z-50}^{FEM}/\sigma_{z-un}^{FEM}$, $\sigma_{z-100}^{FEM}/\sigma_{z-un}^{FEM}$ are also in the parenthesis just below the value of σ_{z-0}^{FEM}, σ_{z-50}^{FEM}, σ_{z-100}^{FEM}, respectively.

From Table 7, the following relation in Eq. (1) can be seen.

$$\frac{\sigma_{z-\sigma_p}^{FEM}}{\sigma_{z-un}^{FEM}} = \frac{F_{1-\sigma_p}^{FEM}}{F_{1-un}^{FEM}} \left(= \frac{K_{1-\sigma_p}^{FEM}}{K_{1-un}^{FEM}} \right) \tag{1}$$

where $\sigma_{z-\sigma_p}^{FEM}$ denotes the stress at the crack tip (see Fig. 14) in the FEM calculation and $F_{1-\sigma_p}^{FEM}$, $K_{1-\sigma_p}^{FEM}$ denote the SIFs of the specimens repaired with CFRP under prestress σ_p. Eq. (1) means that the FEM stress ratio at the crack tip agrees well with the SIF ratio obtained by the contour integral method. Eq. (1) suggests that the FEM stress ratio is useful for expressing the SIF ratio since only the stress value at the crack tip is focused without considering the integral path.

In the previous studies, the relation between the FEM stress at the crack tip (for example σ_{z-un}^{FEM} in Eq. (1)) and the exact SIF (for example K_{1-un}^{EXACT} in Eq. (2)) was investigated for various crack problems when the same FEM mesh is applied. Then, it was found that the FEM stress ratio is mesh-independent and coincide with the ratio of the exact SIF of repaired plate to the exact solution of unrepaired plate, as shown in Eq. (2) if the same FEM mesh is applied (Nisitani et al., 1999, 2004).

$$\frac{\sigma_{z-\sigma_p}^{FEM}}{\sigma_{z-un}^{FEM}} = \frac{F_{1-\sigma_p}^{EXACT}}{F_{I-un}^{EXACT}} \tag{2}$$

The relation (1) was found to be useful for calculating SIFs accurately and conveniently since we can just focus the FEM crack tip stress without considering the contour integral. From Eq. (1) and Eq. (2), we have Eq. (3).

$$\frac{F_{1-\sigma_p}^{FEM}}{F_{1-un}^{FEM}} = \frac{F_{1-\sigma_p}^{EXACT}}{F_{I-un}^{EXACT}} \tag{3}$$

In this way, based on the proportional stress filed relations (2), (3) between the FEM and real ones, the exact SIF of cracked steel plates repaired with prestressed CFRP can be obtained as

Table 7
The dimensionless SIF and the FEM stress value at the crack tip of the unrepaired/repaired specimens.

$2a/W$	F_{1-un}^{FEM}	σ_{z-un}^{FEM}/MPa	F_{1-0}^{FEM} ($\frac{F_{1-0}^{FEM}}{F_{1-un}^{FEM}}$)	σ_{z-0}^{FEM} ($\frac{\sigma_{z-0}^{FEM}}{\sigma_{z-un}^{FEM}}$)	F_{1-50}^{FEM} ($\frac{F_{1-50}^{FEM}}{F_{1-un}^{FEM}}$)	σ_{z-50}^{FEM} ($\frac{\sigma_{z-50}^{FEM}}{\sigma_{z-un}^{FEM}}$)	F_{1-100}^{FEM} ($\frac{F_{1-100}^{FEM}}{F_{1-un}^{FEM}}$)	σ_{z-100}^{FEM} ($\frac{\sigma_{z-100}^{FEM}}{\sigma_{z-un}^{FEM}}$)
0.1000	1.070	975.5	0.9724 (0.9092)	890.9 (0.9132)	0.9475 (0.8859)	868.3 (0.8901)	0.9226 (0.8627)	845.7 (0.8670)
0.2000	1.075	1389	0.9325 (0.8676)	1210 (0.8714)	0.9083 (0.8451)	1179 (0.8489)	0.8841 (0.8226)	1148 (0.8264)
0.6000	1.247	2801	0.8861 (0.7103)	1998 (0.7133)	0.8618 (0.6908)	1944 (0.6938)	0.8378 (0.6716)	1890 (0.6746)
0.7714	1.474	3753	0.9500 (0.6447)	2429 (0.6472)	0.9243 (0.6273)	2364 (0.6299)	0.8986 (0.6098)	2290 (0.6102)

The SIF ratio ≈ the FEM stress can be seen as $\frac{F_{1-0}^{FEM}}{F_{1-un}^{FEM}} \approx \frac{\sigma_{z-0}^{FEM}}{\sigma_{z-un}^{FEM}}$, $\frac{F_{1-50}^{FEM}}{F_{1-un}^{FEM}} \approx \frac{\sigma_{z-50}^{FEM}}{\sigma_{z-un}^{FEM}}$, $\frac{F_{1-100}^{FEM}}{F_{1-un}^{FEM}} \approx \frac{\sigma_{z-100}^{FEM}}{\sigma_{z-un}^{FEM}}$.

$F_{1-\sigma_p}^{EXACT} = F_{1-un}^{EXACT}(\sigma_{z-\sigma_p}^{FEM}/\sigma_{z-un}^{FEM})$ or $F_{1-\sigma_p}^{EXACT} = F_{1-un}^{EXACT}(F_{1-\sigma_p}^{FEM}/F_{1-un}^{FEM})$.

The SIF F_{1-un}^{FEM} in Fig. 6 and the SIF F_{1-0}^{FEM} in Fig. 7 obtained by the contour integral method is shown in Table 8. The central crack plate specimen is often used for fatigue experiment and the SIF can be provided as the following Eq. (4). The previous studies showed that the Eq. (4) can be used as the exact reference solution especially in the range $a/W \leq 0.7714$ in Table 8 considered in this study (Brown and Srawley, 1966; Feddersen, 1966; Isida, 1973).

$$K_{1-un}^{EXACT} = \sigma\sqrt{\pi a}F_{1-un}^{EXACT}$$
$$F_{1-un}^{EXACT} = \left[1 - 0.025\left(\frac{2a}{W}\right)^2 + 0.06\left(\frac{2a}{W}\right)^4\right]\sqrt{\sec\left(\frac{\pi a}{W}\right)} \quad 0 \leq \frac{2a}{W} < 1 \tag{4}$$

The difference of F_{1-un}^{EXACT} and F_{1-un}^{FEM} can be regarded as the FEM error caused by the mesh in Fig. 14 as discussed in Fig. 15. Since the same FEM mesh is applied to analyzing the specimen repaired by CFRP, the same error can be expected for the value of F_{1-0}^{FEM}. Therefore, by applying Eq. (3) based on the proportional stress fields (Oda et al., 2009, 2012), the exact vale of the SIF for repaired specimen can be obtained and indicated as F_{1-0}^{EXACT} in Table 8.

3. Rigorous SIF-based fatigue life prediction of cracked plate repaired by prestressed CFRP

3.1. The fitting equation for SIF

Based on the joint utilization of finite element analysis and the proportionality method, the SIFs of the repaired structures in different prestressing states were obtained. The exact SIF for various prestress σ_p, F_{1-0}^{EXACT}, F_{1-10}^{EXACT}, F_{1-20}^{EXACT}, F_{1-30}^{EXACT}, F_{1-40}^{EXACT}, F_{1-50}^{EXACT}, F_{1-80}^{EXACT}, F_{1-100}^{EXACT} obtained from $F_{1-\sigma_p}^{EXACT} = F_{1-un}^{EXACT}(F_{1-\sigma_p}^{FEM}/F_{1-un}^{FEM})$ are summed up in Table 9. From Table 9, it is seen that the SIFs of the repaired plate with the prestress σ_p = 0, 10, 20, 30, 40, 50, 80 and 100 MPa are much smaller than the SIF of the unrepaired plate. For example, when $2a/W = 0.7714$, the SIF with $\sigma_p = 100$ MPa is reduced to about 60 percent of the unrepaired SIF as $F_{1-\sigma_p}^{EXACT} \approx 0.6F_{1-un}^{EXACT}$.

Table 8
The exact SIF F_{1-un}^{EXACT} obtained from Eq. (4) and the exact SIF F_{1-0}^{EXACT}.

$2a/W$	F_{1-un}^{FEM}	F_{1-un}^{EXACT} obtained from Eq. (4)	F_{1-0}^{FEM} ($F_{1-0}^{FEM}/F_{1-un}^{FEM}$)	F_{1-0}^{EXACT} obtained from $= F_{1-un}^{EXACT}\cdot(F_{1-0}^{FEM}/F_{1-un}^{FEM})$
0.1000	1.070	1.006	0.9724 (0.9088)	0.9142
0.1143	1.069	1.008	0.9655 (0.9032)	0.9104
0.1429	1.069	1.012	0.9532 (0.8917)	0.9024
0.2000	1.075	1.024	0.9325 (0.8674)	0.8883
0.2571	1.085	1.041	0.9149 (0.8432)	0.8778
0.3143	1.099	1.064	0.8997 (0.8187)	0.8710
0.3714	1.118	1.092	0.8875 (0.7938)	0.8669
0.4286	1.140	1.128	0.8792 (0.7712)	0.8699
0.4857	1.169	1.173	0.8764 (0.7497)	0.8794
0.5429	1.204	1.230	0.8787 (0.7298)	0.8977
0.6000	1.247	1.303	0.8861 (0.7106)	0.9259
0.6571	1.303	1.397	0.8993 (0.6902)	0.9642
0.7143	1.375	1.522	0.9194 (0.6687)	1.018
0.7714	1.474	1.698	0.9500 (0.6445)	1.095

The exact SIF of the unrepaired plate F_{1-un}^{EXACT} can be expressed as shown in Eq. (4), that is, $F_{1-un}^{EXACT} = [1 - 0.025(2a/W)^2 + 0.06(2a/W)^4]\sqrt{\sec(2a/W)}$, when $2a/W \to 0$, $F_{1-un}^{EXACT} \to 1$ and when $2a/W \to 1$, $F_{1-un}^{EXACT} \to \infty$. As shown in Table 8, F_{1-un}^{EXACT} increases monotonically with increasing the crack length $2a/W$. Instead, the exact value F_{1-0}^{EXACT} of the repaired plate is in the range $0.9142 \leq F_{1-0}^{EXACT} \leq 1.095$ when $0.1 \leq 2a/W \leq 0.7714$. In other words, due to the repairment, the repaired plate specimen can be regarded as a central crack in an infinite plate with $2a/W \to 0$, which can be expressed as $K_{1-\sigma_p}^{EXACT} \approx \sigma\sqrt{\pi a}$. Those results shows that the fatigue life can be improved significantly by the repair as shown in Fig. 13.

With increasing the prestress σ_p, the SIF decreases irrespective of the crack length $2a/W$ are plotted in Fig. 16. Compared to the SIF with σ_p = 0, the SIF with σ_p = 100 MPa can be reduced by several percent. To clarify the prestress effect on the SIF on the SIF, Fig. 17 shows the SIF ratio $F_{1-\sigma_p}^{EXACT}/F_{1-un}^{EXACT}$ versus $2a/W$ for various prestress σ_p. From Fig. 17, it is seen the SIF ratio $F_{1-\sigma_p}^{EXACT}/F_{1-un}^{EXACT}$ decreases linearly with increasing the prestress ratio $\sigma_p/\sigma_{p\ max}$. The SIF ratio $F_{1-\sigma_p}^{EXACT}/F_{1-un}^{EXACT}$ also decreases linearly with increasing the relative crack length $2a/W$ in the range $0.1 \leq 2a/W \leq 0.7714$ as shown in Eq. (5). The coefficient of determination (COD) of the fitting expression was very close to 1, indicating that the fitting quality is very high.

$$F_{1-\sigma_p}^{EXACT} \Big/ F_{1-un}^{EXACT} = 0.945 - 0.387\left(\frac{2a}{W}\right) - 0.0414\left(\frac{\sigma_p}{\sigma_{p\ max}}\right) \tag{5a}$$

In other words, $F_{1-\sigma_p}^{EXACT}$ can be expressed as follows.

$$K_{1-\sigma_p}^{EXACT} = F_{1-\sigma_p}^{EXACT}\sigma\sqrt{\pi a}$$
$$F_{1-\sigma_p}^{EXACT} = \left[0.945 - 0.387\left(\frac{2a}{W}\right) - 0.0414\left(\frac{\sigma_p}{\sigma_{p\ max}}\right)\right]\times \left[1 - 0.025\left(\frac{2a}{W}\right)^2 + 0.06\left(\frac{2a}{W}\right)^4\right]\sqrt{\sec\left(\frac{\pi a}{W}\right)} \tag{5b}$$
$$0.1 \leq \frac{2a}{W} \leq 0.7714, 0 \leq \frac{\sigma_p}{\sigma_{p\ max}} \leq 1, \sigma_{p\ max} = 100\text{MPa}$$

where $K_{1-\sigma_p}^{EXACT}$ is the SIFs of steel plate repaired with prestressed CFRP (Unit: MPa•m$^{1/2}$), σ_P is the prestress (Unit: MPa), σ_{pmax} is the maximum of cycle load (Unit: MPa), a is the half crack length (Unit: mm), W is the width of steel plate (Unit: mm).

3.2. The prediction of fatigue life

Obtaining the equation for calculating SIF of cracked steel plates repaired with prestressed CFRP is the first step in gaining an equation for fatigue life prediction. The difference between $F_{1-\sigma_p}^{EXACT}$ and F_{1-un}^{EXACT} is quite large up to about 60% at most, as shown in Table 9 and Fig. 16. However, Fig. 17 shows that the ratio $F_{1-\sigma_p}^{EXACT}/F_{1-un}^{EXACT}$ can be used conveniently to express $F_{1-\sigma_p}^{EXACT}$. Since the SIF of the cracked plate repaired by prestressed CFRP can be obtained in a convenient form as shown in Eq. (5), the fatigue life improvement can be predicted in the following way. It is known that fatigue crack propagation can be classified into three stages based on fracture mechanics, that is, crack initiation period, stable crack growth and unstable crack growth. The Pairs-Erdogan equation can be used to describe the stable extension stage as can be expressed in Eq. (6) (Paris and Erdogan, 1963).

$$\frac{da}{dN} = C(\Delta K)^m \tag{6}$$

$$\Delta K = K_{\max} - K_{\min} = (1-R)K_{\max}, R = K_{\min}/K_{\max} \tag{7}$$

Table 9
The exact SIF F_{1-0}^{EXACT}, F_{1-10}^{EXACT}, F_{1-20}^{EXACT}, F_{1-30}^{EXACT}, F_{1-40}^{EXACT}, F_{1-50}^{EXACT}, F_{1-80}^{EXACT}, F_{1-100}^{EXACT} for various prestress σ_p.

$2a/W$	F_{1-un}^{EXACT}	F_{1-0}^{EXACT}	F_{1-10}^{EXACT}	F_{1-20}^{EXACT}	F_{1-30}^{EXACT}	F_{1-40}^{EXACT}	F_{1-50}^{EXACT}	F_{1-80}^{EXACT}	F_{1-100}^{EXACT}
0.1000	1.006	0.9142	0.9099	0.9053	0.9006	0.8959	0.8912	0.8772	0.8678
0.1143	1.008	0.9104	0.9059	0.9012	0.8965	0.8918	0.8872	0.8731	0.8637
0.1429	1.012	0.9024	0.8981	0.8934	0.8887	0.8840	0.8794	0.8653	0.8560
0.2000	1.024	0.8883	0.8843	0.8797	0.8750	0.8704	0.8658	0.8520	0.8428
0.2571	1.041	0.8778	0.8733	0.8688	0.8642	0.8597	0.8552	0.8415	0.8324
0.3143	1.064	0.8710	0.8660	0.8615	0.8570	0.8525	0.8480	0.8346	0.8257
0.3714	1.092	0.8669	0.8629	0.8585	0.8540	0.8495	0.8450	0.8316	0.8227
0.4286	1.128	0.8699	0.8651	0.8606	0.8560	0.8515	0.8469	0.8334	0.8244
0.4857	1.173	0.8794	0.8750	0.8702	0.8654	0.8608	0.8561	0.8420	0.8327
0.5429	1.230	0.8977	0.8933	0.8884	0.8835	0.8788	0.8739	0.8592	0.8496
0.6000	1.303	0.9259	0.9203	0.9152	0.9100	0.9050	0.8999	0.8848	0.8749
0.6571	1.397	0.9642	0.9581	0.9528	0.9476	0.9423	0.9370	0.9214	0.9109
0.7143	1.522	1.018	1.012	1.007	1.001	0.9958	0.9902	0.9738	0.9625
0.7714	1.698	1.095	1.089	1.083	1.077	1.071	1.065	1.047	1.035

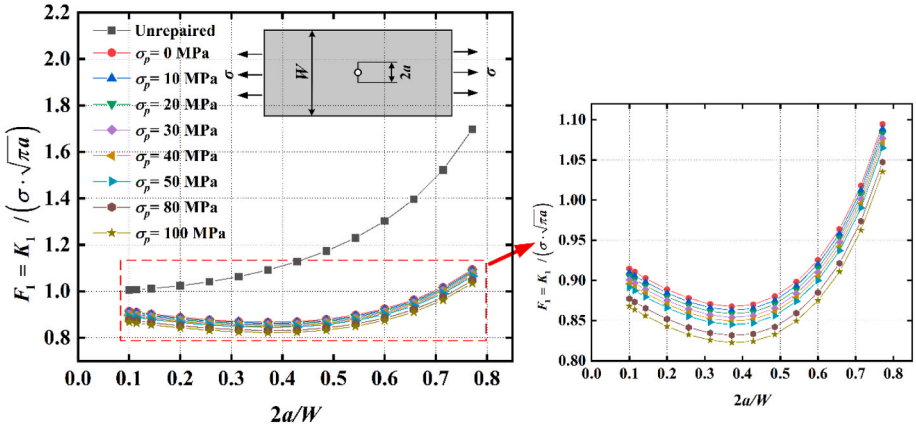

Fig. 16. The exact SIF of the unrepaired plate F_{1-un}^{EXACT} and the repaired plate $F_{1-\sigma_p}^{EXACT}$ with various prestress σ_p = 0, 10, 20, 30, 40, 50, 80 and 100 MPa.

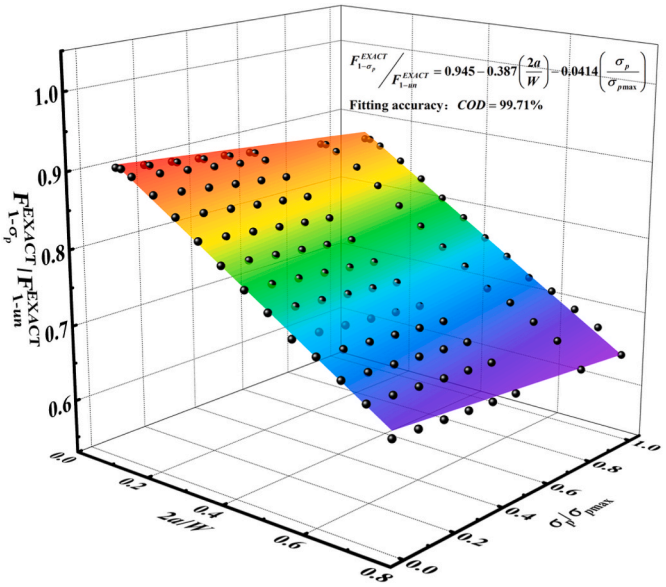

Fig. 17. The exact SIF ratio $F_{1-\sigma_p}^{EXACT}/F_{1-un}^{EXACT}$ for various prestress σ_p = 0, 10, 20, 30, 40, 50, 80 and 100 MPa.

where da/dN is the fatigue crack growth rate, ΔK is the stress intensity factor range. K_{max}, K_{min} are maximum and minimum stress intensity factors in a load cycle, R is the stress ratio. In Eq. (6), C and m are material constants depending on R, obtained from the log-log pot of Eq. (6).

The beach marking method was employed to record fatigue crack growth in experiments, the ASTM E647-15 (2016) indicated Secant method can determine the crack growth rate at each section recorded in testing. The formula is as follows:

$$\left(\frac{da}{dN}\right)_i = \frac{a_{i+1} - a_i}{N_{i+1} - N_i} \tag{8}$$

where a_i and a_{i+1} is the experimentally determined ith and i+1st crack lengths; N_i and N_{i+1} is the number of load cycles corresponding to a_i and a_{i+1}, respectively. Since there were two specimens of cracked steel in both repair stages in the tests, both a and N were calculated as the average of the two specimens' observations. The average crack growth rate is determined by Eq. (8).

The log-log plot of $(da/dN)_i$ - $(\Delta K)i$ relations for i = 1–6 is plotted in Fig. 18, and the linear relation can be seen except the last plots i = 6 of unrepaired plate. Although the crack propagation rates da/dN of unrepaired plate is slightly larger than da/dN of repaired plate, they can be expressed by the same equation within ±5.01% except the last plots i = 6 of unrepaired plate that is not on the linear relation. The equation to express the relation can be determined through intercepting and fitting the experimental data of the stable crack extension process. Then, $C = 6.670 \times 10^{-14}$, m = 3.03 are obtained.

Since Eq. (6) can be expressed as $\int dN = \int 1/[C(\Delta K)^m]da$, the number of cycles N can be expressed in Eq. (9) and Eq. (10) by substituting C and m into Eq. (6) using Eq. (4) and Eq. (5).

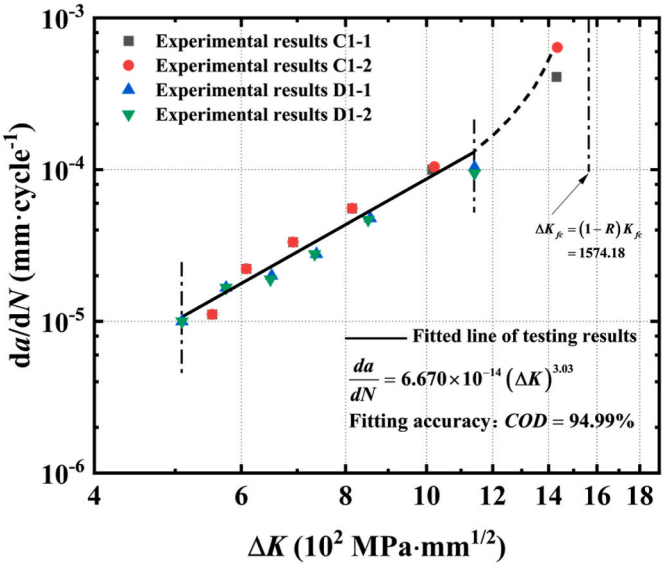

Fig. 18. (da/dN)-(ΔK) plots expressed as $da/dN = C(\Delta K)^m$, $C = 6.670 \times 10^{-14}$, $m = 3.03$ for the stable crack extension stage.

$$N_{c-un} = \int_{a_0}^{a_{c-un}} \frac{da}{C\left[(1-R)K_{1-un}^{EXACT}\right]^m} \quad C = 6.670\times10^{-14}, m = 3.03 \tag{9a}$$

$$K_{1-un}^{EXACT} = \left[1 - 0.025\left(\frac{2a}{W}\right)^2 + 0.06\left(\frac{2a}{W}\right)^4\right]\sqrt{\sec\left(\frac{\pi a}{W}\right)}\sigma\sqrt{\pi a} \tag{9b}$$

$$N_{c-\sigma_P} = \int_{a_0}^{a_{c-0}} \frac{da}{C\left[(1-R)K_{1-\sigma_P}^{EXACT}\right]^m} \quad C = 6.670\times10^{-14}, m = 3.03 \tag{10a}$$

$$K_{1-\sigma_P}^{EXACT} = \left[0.945 - 0.387\left(\frac{2a}{W}\right) - 0.0414\left(\frac{\sigma_p}{\sigma_{p\ \max}}\right)\right]\times \left[1 - 0.025\left(\frac{2a}{W}\right)^2 + 0.06\left(\frac{2a}{W}\right)^4\right]\sqrt{\sec\left(\frac{\pi a}{W}\right)}\sigma\sqrt{\pi a} \tag{10b}$$

This equation can be used to rapidly calculate the fatigue life of Q235 steel plates with central cracks repaired by CFRP without or with different prestress, and this method can be applied to CRPP repairing plates with different materials, but the critical crack length should be known in advance to obtain fatigue life. Eq. (9) is defined up to the final crack length $2a_{c\text{-}un} = 44.10$ mm and Eq. (10) is defined up to $2a_{c\text{-}0} = 53.0$ mm (see Table 5). From these final fatigue crack lengths where unstable fracture happens, the fatigue fracture toughness can be calculated for the unrepaired steel plate as $K_{fc} = 63.02$ MPa $m^{1/2}$ and for the repaired steel plate as $K_{fc} = 55.31$ MPa $m^{1/2}$ (see Table 5). Those values nearly coincide with each other within 12.24% difference. They are obtained under cyclic load and smaller than the fracture toughness obtained by a monotonic load $K_{fc} < K_c = 83.16$ MPa $m^{1/2}$ in Table 1. The difference of K_{fc} between the unrepaired and repaired plates can be explained by the spread of the peeling area of the CFRP repaired plate. This is because FEA always assumes a perfect bond until the final fracture yet crack opening and closing during cyclic loading may cause the peeling.

The basic form of the fatigue life prediction equation of unrepaired and repaired steel plates can be obtained by jointly using the rigorous SIF equation and the Paris-Erdogan equation. Eqs. (9) and (10) are defined from the initial crack length $2a_0 = 7.0$ mm to the final crack lengths $2a_{c\text{-}un} = 44.10$ mm, $2a_{c\text{-}0} = 53.0$ mm; therefore, $N_{c\text{-}un}$, $N_{c\text{-}\sigma p}$ are regarded as the number of cycles to failure for unrepaired and repaired steel plates. In this way, the fatigue crack length versus number of cycle (a-N relation) can be provided. Fig. 19 shows the results of Eqs. (9) and (10) with $C = 6.670 \times 10^{-14}$, $m = 3.03$ in comparison with the experimental results. Eq. (9) provides relatively larger value of fatigue life for the unrepaired plates; its difference is 7.81% compared to the experimental results. Eq. (10) predicts the fatigue life of the CFRP repaired plate with less than 5.50% difference.

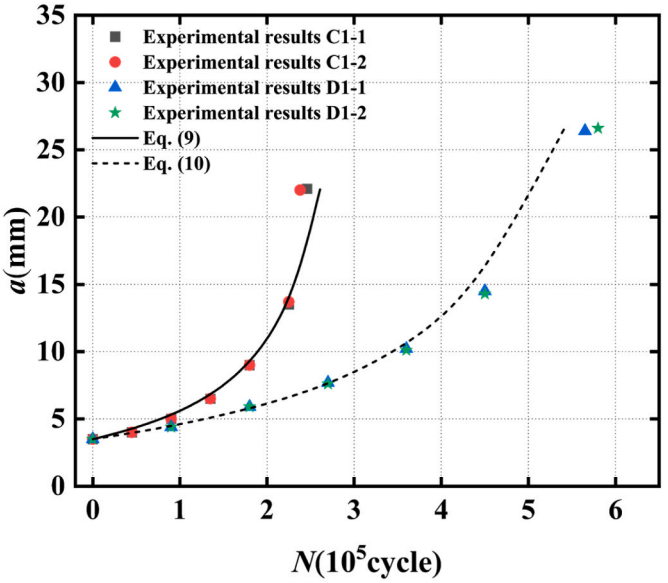

Fig. 19. Fatigue crack length versus number of cycles (a-N relation) obtained from Eqs. (9) and (10) compared to the experimental results in Fig. 13.

The predicted crack length (a-N relation) obtained from Eqs. (9) and (10) to clarify the effect of prestress are presented in Fig. 20. It should be mentioned that experiments are required for obtaining the final crack length of the repaired steel with prestressed CFRP. Nevertheless, the experiment was not carried out in this investigation.

. To evaluate how prestress affects fatigue life, the experimental ultimate crack length of steel plates repaired with common CFRP was employed as the referenced value. Fig. 20 shows that the fatigue life

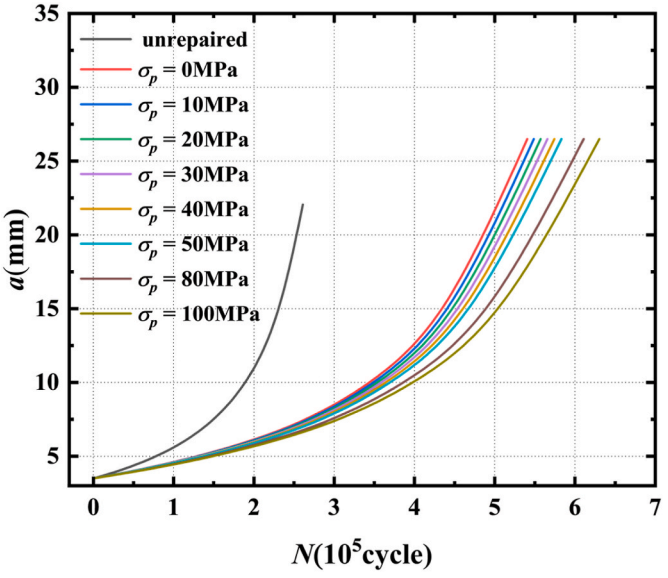

Fig. 20. Fatigue crack length versus number of cycles (a-N relation) obtained from Eqs. (9) and (10).

N_c can be extended by 2.07–2.41 times by repairing with the prestressed CFRP.

4. Conclusions

Cracked plates in steel structures are now widely repaired by prestressed CFRP. The safety and reliability of the repair are depending on their fatigue performance. In this study, first, the fatigue experiment was conducted for the unrepaired/repaired plates. Second, the SIF of the cracked plate with/without repair was calculated by using a standard FEM software. Third, the error due to the FEM mesh was evaluated by comparing with the exact solution for the unrepaired plate. Finally, the fatigue life extension was predicted for the cracked steel plate repaired by various prestressed CFRP. The conclusions can be summarized in the following way.

(1) It was found that the error of the SIFs included in the FEA using a commercial software can be eliminated on the idea of the proportional method. The crack tip FEM stress ratio which was focused in the previous proportional method coincides with the FEM SIF ratio obtained by the finite element software when the same FEM mesh is applied to the unknown and reference problems. Since by taking the ratio the FEM mesh error is eliminated, the exact SIF of repaired plate can be provided from the exact solution of unrepaired plate and the FEM ratio.

(2) It was found that the SIF ratio $F^{EXACT}_{1-\sigma_p}/F^{EXACT}_{1-un}$ of the repaired plate to the unrepaired plate decreases linearly with increasing the prestress $\sigma_p/\sigma_{p\ \max}$ in CFRP. The SIF ratio $F^{EXACT}_{1-\sigma_p}/F^{EXACT}_{1-un}$ also decreases linearly with increasing the relative crack length $2a/W$ as can be expressed in Eq. (5). Although the difference between $F^{EXACT}_{1-\sigma_p}$ and F^{EXACT}_{1-un} is quite large up to 60 % at most it was found that the ratio $F^{EXACT}_{1-\sigma_p}/F^{EXACT}_{1-un}$ can be used conveniently to express $F^{EXACT}_{1-\sigma_p}$. The exact SIF expression (5) combined with Paris-Erdogan's law may predict the fatigue life of the repaired plate within 5.50% difference as shown in Fig. 19. The fatigue life N_c can be extended by about two times longer by repairing the cracked steel plate with the prestressed CFRP.

(3) The crack propagation rate experimentally obtained for unrepaired/repaired plates can be expressed by almost the same equation (see Fig. 19). Also, the fatigue fracture toughness of the unrepaired steel plate nearly coincides with the fatigue fracture toughness of repaired steel plate within 12.24% difference (see Table 5). The difference of K_{fc} between the unrepaired and repaired plates can be explained from that the possible spread of the peeling area of the CFRP repair plate. This is because FEA always assumes a perfect bond until the final fracture, yet crack opening and closing occurs during cyclic loading.

CRediT authorship contribution statement

Yu Zhang: Conceptualization, Methodology, Validation, Formal analysis, Investigation, Visualization, Resources, Writing – review & editing, Supervision, Project administration, Funding acquisition. **Feifan Zhang:** Software, Validation, Formal analysis, Investigation, Data curation, Writing – original draft, Writing – review & editing. **Zhansheng Guo:** Validation, Investigation, Software. **Nao-Aki Noda:** Formal analysis, Writing – review & editing.

Declaration of competing interest

The authors declare that they have no known competing financial interests or personal relationships that could have appeared to influence the work reported in this paper.

Data availability

Data will be made available on request.

References

Abaqus, 2020. ABAQUS Version 2020. Dessault Syst.

Aljabar, N.J., Zhao, X.L., Al-Mahaidi, R., Ghafoori, E., Motavalli, M., Koay, Y.C., 2018. Experimental investigation on the CFRP strengthening efficiency of steel plates with inclined cracks under fatigue loading. Eng. Struct. 172, 877–890. https://doi.org/10.1016/j.engstruct.2018.06.074.

Al-Karawi, H., Polach, R.U.F., von, B. und, Al-Emrani, M., 2020. Fatigue crack repair in welded structures via tungsten inert gas remelting and high frequency mechanical impact. J. Constr. Steel Res. 172, 12. https://doi.org/10.1016/j.jcsr.2020.106200.

Al-Mosawe, A., Al-Mahaidi, R., Zhao, X.L., 2016. Bond behaviour between CFRP laminates and steel members under different loading rates. Compos. Struct. 148, 236–251. https://doi.org/10.1016/j.compstruct.2016.04.002.

ASTM E647-15, 2016. Standard Test Method for Measurement of Fatigue Crack Growth Rates. ASTM International, West Conshohocken, United States.

Batuwitage, C., Fawzia, S., Thambiratnam, D., Al-Mahaidi, R., 2017. Durability of CFRP strengthened steel plate double-strap joints in accelerated corrosion environments. Compos. Struct. 160, 1287–1298. https://doi.org/10.1016/j.compstruct.2016.10.101.

Brown, W.F., Srawley Jr., 1966. J. Plane Strain Crack Toughness Testing of High Strength Metallic Materials. ASTM STP-410, p. 11.

Cabrilo, A., Sedmak, A., Burzic, Z., Perkovic, S., 2019. Fracture mechanics and fatigue crack propagation in armor steel welds. Eng. Fail. Anal. 106, 104155 https://doi.org/10.1016/j.engfailanal.2019.104155.

Chen, T., Yao, J.X., Liu, R.Y., Li, L.Z., 2020. Fatigue behavior of steel plates with multi-holes repaired by CFRP. Compos. Struct. 242, 112163 https://doi.org/10.1016/j.compstruct.2020.112163.

Colombi, P., Fava, G., 2016. Fatigue crack growth in steel beams strengthened by CFRP strips. Theor. Appl. Fract. Mech. 85, 173–182. https://doi.org/10.1016/j.tafmec.2016.01.007.

Deng, J., Fei, Z., Wu, Z., Li, J., Huang, W., 2023. Integrating SMA and CFRP for fatigue strengthening of edge-cracked steel plates. J. Constr. Steel Res. 206, 107931 https://doi.org/10.1016/j.jcsr.2023.107931.

Dong, D.S., Mei, X., 2003. Testing for paris coefficients C, m and ΔK_{th} of Q235. J. Mech. Strength 215–218. https://doi.org/10.16579/j.issn.1001.9669.2003.02.025, 02.

Feddersen, R.E., 1966. Discussion to the above Paper. ASTM STP-410, p. 77.

Feng, P., Hu, L.L., Zhao, X.L., Cheng, L., Xu, S.H., 2014. Study on thermal effects on fatigue behavior of cracked steel plates strengthened by CFRP sheets. Thin-Walled Struct. 82, 311–320. https://doi.org/10.1016/j.tws.2014.04.015.

Hassan, M.M., Shafiq, M.A., Mourad, S.A., 2021. Experimental study on cracked steel plates with different damage levels strengthened by CFRP laminates. Int. J. Fatig. 142, 105914 https://doi.org/10.1016/j.ijfatigue.2020.105914.

Isida, M., 1973. Eng. Fract. Mech. 5, 647–665.

Jie, Z.Y., Wang, W.J., Fang, R.F., Zhuge, P., Ding, Y., 2020. Stress intensity factor and fatigue analysis of cracked cruciform welded joints strengthened by CFRP sheets considering the welding residual stress. Thin-Walled Struct. 154, 106818 https://doi.org/10.1016/j.tws.2020.106818.

Kafodya, I., Xian, G.J., Li, H., 2015. Durability study of pultruded CFRP plates immersed in water and seawater under sustained bending: water uptake and effects on the mechanical properties. Composer Part B-Eng. 70, 138–148. https://doi.org/10.1016/j.compositesb.2014.10.034.

Lepretre, E., Chataigner, S., Dieng, L., Gaillet, L., 2021. Stress intensity factor assessment for the reinforcement of cracked steel plates using prestressed or non-prestressed adhesively bonded CFRP. Materials 14, 1625. https://doi.org/10.3390/ma14071625.

Li, L.Z., Chen, T., Zhang, N.X., Hidekuma, Y., 2019. Test on fatigue repair of central inclined cracked steel plates using different adhesives and CFRP, prestressed and non-prestressed. Compos. Struct. 216, 350–359. https://doi.org/10.1016/j.compstruct.2019.03.012.

Li, Y., Lu, P., Wang, B., Hu, X., Li, D., Xiang, Q., 2022. Evaluation of the fracture toughness of butt-welded joints using the boundary effect model. Eng. Fract. Mech. 274, 108777 https://doi.org/10.1016/j.engfracmech.2022.108777.

Liu, H., Al-Mahaidi, R., Zhao, X., 2009. Experimental study of fatigue crack growth behaviour in adhesively reinforced steel structures. Compos. Struct. 90, 12–20. https://doi.org/10.1016/j.compstruct.2009.02.016.

Liu, J., Zhao, X.-L., Xin, H., Zhang, Y., 2023. Prediction of fatigue crack propagation in center cracked steel plate strengthened with partially covered CFRP strip. Thin-Walled Struct. 189, 110917 https://doi.org/10.1016/j.tws.2023.110917.

Liu, R.Y., Chen, T., Li, L.Z., Tateishi, K., 2019. A practical stress intensity factor formula for CFRP-repaired steel plates with a central crack. J. Constr. Steel Res. 162, 105755 https://doi.org/10.1016/j.jcsr.2019.105755.

Liu, Z.Q., Luo, B., Wang, Q., Feng, B., 2021. Experimental and numerical investigation of the anti-debonding performance for novel CFRP-steel tube composite member under tension. J. Build. Eng. 35, 102004 https://doi.org/10.1016/j.jobe.2020.102004.

Mazaheri, P., Asgarian, B., Gholami, H., 2021. Assessment of strengthening, modification, and repair techniques for aging fixed offshore steel platforms. Appl. Ocean Res. 110, 102612 https://doi.org/10.1016/j.apor.2021.102612.

Nisitani, H., Teranishi, T., 2004. KI of a circumferential crack emanating from an ellipsoidal cavity obtained by the crack tip stress method in FEM. Eng. Frac.t Mech.

Fracture and Damage Mechanics 71, 579–585. https://doi.org/10.1016/S0013-7944(03)00035-3.
Nisitani, H., Kawamura, T., Fujisaki, W., Fukuda, T., 1999. Determination of highly accurate values of stress intensity factor or stress concentration factor of plate specimen by FEM. J-STAGE. A 65, 26–31. https://doi.org/10.1299/KIKAIA.65.26.
Oda, K., Kamisugi, K., Noda, N., 2009. Analysis of stress intensity factor for interface cracks based on proportional method. Nihon Kikai Gakkai Ronbunshu, J-STAGE. A75, 476–482. https://doi.org/10.1299/kikaia.75.476.
Oda, K., Lan, X., Noda, N., Michinaka, K., 2012. Effect of arbitrary bi-material combination and bending loading conditions on stress intensity factors of an edge interface crack. Int. J. Struct. Integr. 3, 457–475. https://doi.org/10.1108/17579861211281236.
Orcesi, A.D., Feraille, A., Chataigner, S., 2019. Fatigue strengthening of steel structures using high modulus CFRP plates: development of a life-cycle analysis approach. Construct. Build. Mater. 227, 116628 https://doi.org/10.1016/j.conbuildmat.2019.08.009.
Pang, Y.Y., Wu, G., Wang, H.T., Su, Z.L., He, X.Y., 2019. Experimental study on the bond behavior of CFRP-steel interfaces under quasi-static cyclic loading. Thin-Walled Struct. 140, 426–437. https://doi.org/10.1016/j.tws.2019.03.060.
Paris, P., Erdogan, F., 1963. A critical analysis of crack propagation laws. J. Basic Eng. 85, 528–533. https://doi.org/10.1115/1.3656900.
Russian, O., Belarbi, A., Dawood, M., 2022. Effect of surface preparation technique on fatigue performance of steel structures repaired with self-stressing SMA/CFRP patch. Compos. Struct. 280, 114968 https://doi.org/10.1016/j.compstruct.2021.114968.
Shao, W., Wang, Y., Shi, D., 2022. Corrosion-fatigue life prediction of reinforced concrete square piles in marine environments. Eng. Fail. Anal. 138, 106324 https://doi.org/10.1016/j.engfailanal.2022.106324.
Täljsten, B., Hansen, C.S., Schmidt, J.W., 2009. Strengthening of old metallic structures in fatigue with prestressed and non-prestressed CFRP laminates. Construct. Build. Mater. 23, 1665–1677. https://doi.org/10.1016/j.conbuildmat.2008.08.001.
Tan, H., Hu, X., Wu, X., Zeng, Y., Tu, X., Xu, X., Qian, J., 2021. Initial crack propagation of integral joint in steel truss arch bridges and its fatigue life accession. Eng. Fail. Anal. 130, 105777 https://doi.org/10.1016/j.engfailanal.2021.105777.
Wang, H.T., Bian, Z.N., Chen, M.S., Hu, L., Wu, Q., 2023. Flexural strengthening of damaged steel beams with prestressed CFRP plates using a novel prestressing system. Eng. Struct. 284, 115953 https://doi.org/10.1016/j.engstruct.2023.115953.
Weitzenboeck, J.R., Mcgeorge, D., 2012. A Cold Repair Method for FPSOs. Presented at the Offshore Technology Conference, Houston, Texas, USA. https://doi.org/10.4043/23543-MS.
Wu, C., Zhao, X.L., Al-Mahaidi, R., Emdad, M.R., Duan, W.H., 2012. Fatigue tests of cracked steel plates strengthened with UHM CFRP plates. Adv. Struct. Eng. 15, 1801–1815. https://doi.org/10.1260/1369-4332.15.10.1801.
Xue, W.C., Tan, Y., Zeng, L., 2010. Flexural response predictions of reinforced concrete beams strengthened with prestressed CFRP plates. Compos. Struct. 92, 612–622. https://doi.org/10.1016/j.compstruct.2009.09.036.
Yu, Q.Q., Zhao, X.L., Al-Mahaidi, R., Xiao, Z.G., 2014. Tests on cracked steel plates with different damage levels strengthened by CFRP laminates. Int. J. Struct. Stabil. Dynam. 14, 1450018 https://doi.org/10.1142/S0219455414500187.